AAS 13-371

NUMERICAL ANALYSIS OF THERMAL RADIATION PERTURBATIONS FOR A MERCURY ORBITER

Benny Rievers,* Takahiro Kato,†
Jozef van der Ha‡ and Claus Lämmerzahl§

The perturbations induced by solar and thermal radiation are among the major design drivers for the mission design and operation of near-solar space missions. While the magnitude of these perturbations is proportional to the inverse square of the distance to the sun, their effects may vary drastically depending on the orbit and eclipse conditions. Furthermore, the spacecraft configuration, the optical properties as well as the attitude significantly affect the resulting magnitude and direction of the perturbations. Therefore, all of these effects need to be included in a high-fidelity analysis. While analytical methods offer a useful quick first-order assessment of the characteristics of the thermal effects, high-precision predictions can only be achieved by using numerical methods. They are able to incorporate any complicated spacecraft configuration as well as sophisticated environmental properties like, for instance, the thermo-optical properties of a planetary surface. Motivated by this, a numerical approach for the precise modelling of the solar and thermal effects acting on a Mercury Orbiter is presented. The expected disturbances resulting from thermal and solar perturbations are calculated for a Messenger-like mission. Due to the close distance to the sun and the high temperature gradients on the surface of Mercury, the evolving disturbances significantly affect the trajectory of the spacecraft.

INTRODUCTION

Spacecraft orbiting the inner planets of the solar system, in particular Mercury, are subject to considerable perturbations resulting from interactions with the harsh space environment in the vicinity of the sun. The major influence on the trajectory of the spacecraft results from momentum exchange between photons and the spacecraft surfaces. Besides the solar radiation pressure (SRP) acting on the spacecraft surface, the sunlight reflected from the planet surface as well as the emitted planetary infrared radiation result in Albedo pressure (ALB) and Infrared pressure (INF) contributions to the resulting perturbations. Furthermore the thermal radiation emitted by the satellite itself leads to a thermal radiation pressure (TRP), adding up to the total effect.

The importance of an accurate modeling has already been demonstrated by a number of recent publications. With a high precision thermal analysis of the Pioneer 10 spacecraft[1] we have shown, that the so called Pioneer anomaly, a nearly constant deceleration of the probe on its way out of the solar system, is in fact caused by TRP. In that case, the anisotropic dissipation of the radio-isotopic

*Postdoctoral Researcher, Fundamental Physics Department, Center of Applied Space Technology and Microgravity (ZARM), University of Bremen, Am Fallturm, 28359 Bremen, Germany; benny.rievers@zarm.uni-bremen.de
†Postdoctoral Researcher, GNC systems, Institute of Space Systems, German Aerospace Center (DLR), Robert Hooke-Str.7, 28359 Bremen, Germany; Kato.Takahiro@dlr.de
‡Consultant, Europa-Allee 15, 64625 Bensheim, Germany; jvdha@aol.com
§Director General, Center of Applied Space Technology and Microgravity (ZARM), University of Bremen, Am Fallturm, 28359 Bremen, Germany; claus.laemmerzahl@zarm.uni-bremen.de

thermal generator waste heat as well as the spacecraft compartment heat are causing the disturbance.[1] As another example, an analysis of thermal disturbances acting on ESAs Rosetta spacecraft during its heliocentric cruise phases has uncovered a non-modeled thermal drag correlated with the solar radiation pressure which led to roughly 10 % deviation of measured and modeled SRP.[2–5] By using analytical methods we could also show that the treatment of thermal effects is particularly important for missions such as Messenger which operate close to the sun.[6]

The significance of accurate SRP, ALB and INF modelling has also been demonstrated for the case of Messenger by Scott et al.,[7] who used analytical disturbance force models as inputs in numerical orbit propagators and estimated the influence on the orbital elements. Motivated by these results and our own experiences, the scope of this paper is the introduction of a complete generic numerical approach for the calculation of solar and thermal disturbances. This new method yields an improved modeling precision compared to the analytical methods introduced in Kato et al.[6] Furthermore we add a high precision TRP model, which includes thermal interactions between spacecraft and planet, to the set of available numerical disturbance analysis methods.

A high precision numerical approach demands the inclusion of detailed spacecraft geometry, optical properties of the spacecraft surfaces as well as a detailed geometric model of the planet surface. In our approach, the spacecraft as well as the planet are therefore represented by a set of surface cells allowing for the inclusion of geometrical details. The method is implemented by means of a generic MATLAB/SIMULINK-based software tool with a modular structure. This GENERIC tool includes individual models for the solar radiation pressure, the re-emitted thermal radiation pressure and, in addition, for the planetary albedo and infrared radiation pressure effects. Furthermore the orbits of planet and spacecraft are integrated numerically and transformations between different coordinate systems, the calculation of solar eclipse conditions as well as field-of-view computations are included. Starting conditions can either be specified as Keplerian elements or as satellite/planet state vectors thus enabling a broad range of possible input parameter variations. The individual disturbance models as well as the general numerical approach are explained in the following sections.

GENERIC OVERVIEW

The general structure of the GENERIC tool is displayed in figure 1. Three main blocks can be identified. The input section controls the interface to external data such as the planet model, the spacecraft model as well as the user-defined simulation starting options. Here the different models as well as the initial state vectors/ephemeris of planet and spacecraft are specified by the user by means of external text files. The orbit section controls the numerical integration of the planet and spacecraft orbit as well as the transformations between spacecraft, planet and inertial coordinate frames.

The non-gravitational forces section includes the individual SIMULINK disturbance models for SRP, TRP, ALB and INF. The methods described in this paper are implemented by MATLAB s-functions with input/output ports. Here the disturbance models use the info specified in the input section, such as the satellite geometry, satellite optical surface parameters, planet optical surface parameters as well as the state vectors of planet and satellite as basis for the calculation of the resulting orbit perturbations. The different methods used within the individual blocks as well as the basic theory for the calculation of the disturbances are described in the following section.

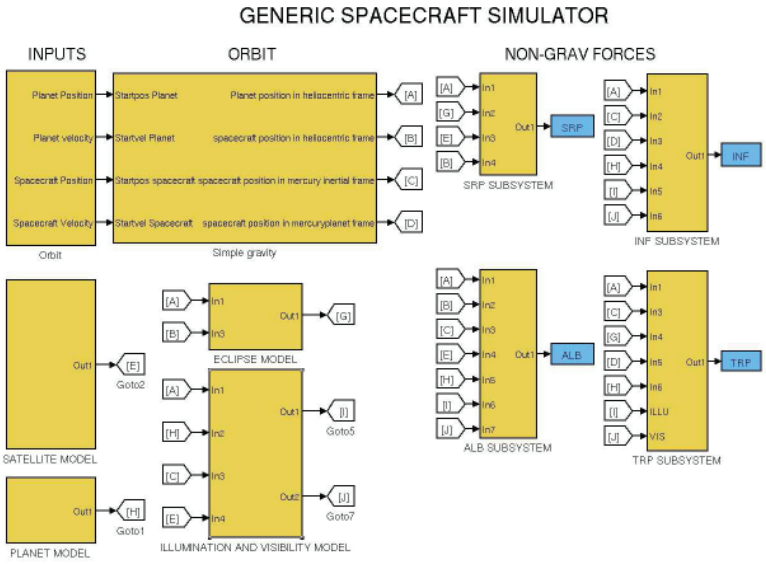

Figure 1. Structure of the GENERIC simulation tool

BASIC EQUATIONS AND MODELS

Coordinate systems

The spacecraft trajectory is mainly determined by the gravitational interaction with Mercury. However, for long-term simulations, the position of the gravitating body also changes with respect to the sun. Since the direction of the sun with respect to spacecraft and planet, as well as the position of the spacecraft relative to the planet dominate the resulting thermal forces, different coordinate systems have to be implemented to describe all relevant effects properly. The GENERIC simulator includes four main coordinate frames:

1. The J2000 Heliocentric inertial frame (subscript HCI),
2. The J2000 Mercurycentric inertial frame (subscript MCI),
3. The planet frame (subscript PL),
4. The spacecraft frame (subscript SC).

As can be seen in figure 2 the HCI is centered within the sun with x_{HCI}-axis pointing to the vernal equinox, z_{HCI}-axis is normal to the ecliptic plane and y_{HCI}-axis is perpendicular to x_{HCI} and z_{HCI}. This inertial frame is used for the numerical integration of the planet trajectory as well as for the determination of the eclipse conditions. This implies that the starting orbital elements of the planet are given within the HCI-frame. The MCI is centered within Mercury, where the x_{MCI}-axis points towards the ascending node of Mercury's orbital plane, the z_{MCI}-axis is normal to Mercury's rotation axis (which is effectively normal to the Mercury orbital plane, due to the negligible axis tilt) and the y_{MCI}-axis is perpendicular to x_{MCI} and z_{MCI}. This inertial frame is used to compute the trajectory of the spacecraft in the planet's inertial coordinates. Consequently the starting orbital elements of the spacecraft are defined within the MCI. The PL system is used for a convenient

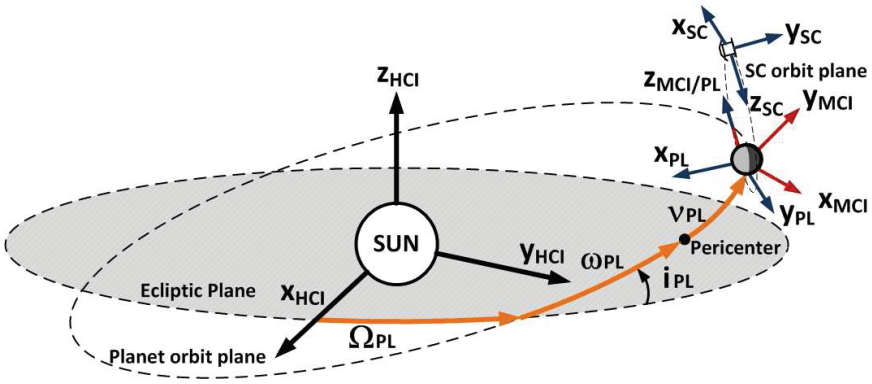

Figure 2. Coordinate frames implemented in GENERIC

formulation of the planet lighting conditions as well as the description of the thermal interactions between planet and spacecraft surfaces. Therefore, the x_{PL}-axis is aligned with the sun direction, z_{PL} is normal to Mercury's orbital plane and y_{PL} is perpendicular to x_{PL} and z_{PL}. The SC frame is implemented to express all computed forces acting on the spacecraft according to the current orientation of the spacecraft itself. It is assumed that within the scope of the studied orbit periods sun-pointing is kept at all times. Consequently y_{SC} is aligned with x_{PL}, while z_{SC} and x_{SC} are kept at the initial orientation of the body height and length axes, respectively, which are assumed to be aligned with $-z_{PL}$ and $-y_{PL}$, respectively. For the assessment of the different effects which depend on the relative position and orientations of the frames, coordinate transformations between all defined frames are needed. The main transformations are described in the following.

The transformation between MCI and HCI, which is needed for an accurate description of the spacecraft position in HCI frame, can be realized by rotating with planet inclination i_{pl} around x_{MCI} and planet right ascension Ω_{pl} around z_{HCI} as well as offsetting with the planet position $\vec{r}_{pl,HCI}$. Here $\underline{\underline{A}}$ denotes a transformation matrix. Consequently the transformation of a vector $\vec{r}_{sc,HCI}$ in MCI frame to HCI frame can be expressed as:

$$\begin{aligned} \vec{r}_{sc,HCI} &= \underline{\underline{A}}_{MCI->HCI} \cdot \vec{r}_{sc,MCI} \qquad (1) \\ &= \begin{bmatrix} \cos\Omega_{pl} & -\sin\Omega_{pl}\cos i_{pl} & \sin\Omega_{pl}\sin i_{pl} \\ \sin\Omega_{pl} & \cos\Omega_{pl}\cos i_{pl} & -\cos\Omega_{pl}\sin i_{pl} \\ 0 & \sin i_{pl} & \cos i_{pl} \end{bmatrix} \cdot \vec{r}_{sc,MCI} + \vec{r}_{pl,HCI} \,. \end{aligned}$$

The transformation between HCI and MCI is described by the inverse of $\underline{\underline{A}}_{MCI->HCI}$. The transformation between MCI and planet frame is governed by the planet argument of periapsis ω_{pl} and the planet true anomaly ν_{pl} as well as the sun-alignment requirement. Consequently the transformation can be expressed by a single rotation around z_{MCI} with:

$$\begin{aligned} \vec{r}_{sc,PL} &= \underline{\underline{A}}_{MCI->PL} \cdot \vec{r}_{sc,MCI} \qquad (2) \\ &= \begin{bmatrix} \cos\phi_{pl} & \sin\phi_{pl} & 0 \\ -\sin\phi_{pl} & \cos\phi_{pl} & 0 \\ 0 & 0 & 1 \end{bmatrix} \cdot \vec{r}_{sc,MCI} \,, \end{aligned}$$

where the position angle ϕ_{pl} is given by

$$\phi_{pl} = \nu_{pl} + \omega_{pl} + \pi \,. \tag{3}$$

The reverse transformation $\underline{\underline{A}}_{PL->MCI}$ is again given by the inverse $\underline{\underline{A}}_{MCI->PL}$. Finally the transformation between planet frame and body frame is given by the alignment criteria as specified above. Thus the transformation can be expressed as:

$$\begin{aligned} \vec{r}_{sc,SC} &= \underline{\underline{A}}_{PL->SC} \cdot \vec{r}_{sc,PL} \\ &= \begin{bmatrix} 0 & -1 & 0 \\ -1 & 0 & 0 \\ 0 & 0 & -1 \end{bmatrix} \cdot \vec{r}_{sc,PL} \,, \end{aligned} \tag{4}$$

which is identical to $\underline{\underline{A}}_{SC->PL}$. All other transformations such as $\underline{\underline{A}}_{HCI->SC}$ can be calculated from combinations of the transformations specified above.

Spacecraft model

In order to implement a realistic model of the spacecraft, we apply a set of surface cells to assemble the complete spacecraft. As listed in table 1, the optical surface parameters as well as the position and the orientation of the respective spacecraft cells need to be specified in the spacecraft frame. The transformation into planet and inertial frame, which is performed within the input block then gives the needed inputs for the calculation of the various perturbations. The total number of surface cells is not limited in this approach and can be chosen freely, corresponding to the required level of detail. With this, the numerical model employs a greatly improved geometric modelling capability compared to analytical models. Note that this approach only allows for external surfaces, since merely the orientation angle of a surface to the source of a perturbation (sun, planet) determines whether the surface is subjected to it. Consequently, a body with a front and a rear side (such as a solar panel) has to be modeled by at least two individual surface cells.

Table 1. Spacecraft model interface

Cell area [m^2]	Right ascension [rad]	Declination [rad]	Cell center [m]	α_{sc}	$\gamma_{S,sc}$	$\gamma_{D,sc}$

Here α_{sc} is the optical coefficient of absorption of the spacecraft surface, $\gamma_{S,sc}$ and $\gamma_{D,sc}$ are the coefficient of specular and diffuse reflection, respectively. A visualization of the spacecraft model interface (Messenger case) is shown in figure 3 left. Note that the right ascension, the declination and the surface center vector have to be specified within the SC-frame.

Planet model

For the calculation of ALB, INF and TRP the radiation exchange between planet and satellite surfaces determines the magnitude of the resulting perturbations. The exchanged radiation fluxes depend on the radiation view factors, which are given by the relative orientation between satellite and planet surfaces and denote the fraction of radiation exchanged between a radiation source and an absorber. Consequently, the accuracy of the calculation of the effects resulting from an interaction with the orbited planet can be increased by also modeling the planet surface as a set of surface cells, since the orientation of the normal direction on the planet surface to the spacecraft cells changes with the position of the spacecraft on its orbit. The planet model is shown in figure 3 right for an

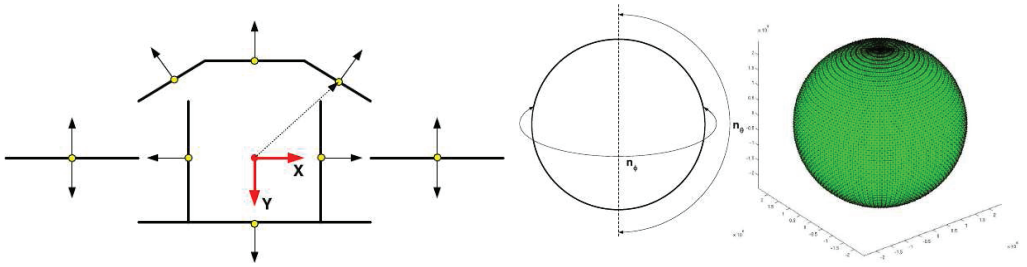

Figure 3. Visualization of spacecraft model interface (left) and planet model interface (right)

exemplary case. As can be seen, the planet is assumed to be an ideal sphere, where the individual surfaces are specified by the angles Φ and Θ, which describe the position of the respective surface elements corner node positions in spherical coordinates and consequently the size of the cell surface. Each surface cell obtains a center node which specifies the considered normal direction (normalized vector between planet center and surface element center). Note that the resolution of the planetary grid can be specified freely, at the cost of computational time for a high number of surface elements. As necessary inputs for the calculation the optical parameters of the planet surface as well as the mean cell temperatures have to be specified as shown in table 2. Note that different values of optical parameters and temperature may be assigned to each cell which, for instance, is used to assign different temperatures on the planets day and night side.

Table 2. Planet model interface

Surface area [m^2]	Right ascension [rad]	Declination [rad]	α_{pl}	$\gamma_{D,pl}$	ε_{pl}

Here α_{pl} is the optical coefficient of absorption of the planet surface cells, $\gamma_{D,pl}$ is the coefficient of diffuse reflection and ε_{pl} is the coefficient of emission. The total number of cells is given by the planet resolution n_{res}, which determines the number of elements n_Φ and n_Θ in Φ and Θ direction by $n_{cells} = 2 \cdot n_{res}^2 = n_\Theta \cdot n_\Phi = 2n_\Theta^2$. The planet cell center coordinates (in planet frame) are determined by

$$\vec{r}_{C,PL}(i,j) = \begin{bmatrix} R_{pl} \cos\Phi(i) \cos\Theta(j) \\ R_{pl} \sin\Phi(i) \cos\Theta(j) \\ R_{pl} \sin\Theta(j) \end{bmatrix} , \tag{5}$$

with planet radius R_{pl}. Here the borders of a specific planet surface cell i, j are given by

$$\Phi(i) = -\pi + 2\pi \cdot (i-1)/n_\Phi \text{ and } \Theta(j) = -\pi/2 + \pi \cdot (j - 1/2)/n_\Theta \,. \tag{6}$$

The normal direction of each planet cell is characterized by the vector norm of $\vec{r}_{C,PL}(i,j)$. The cell surface area is calculated in a twofold approach. First, the surface of a spherical section $A_M(j)$ bordered by the elevation angles $\Theta(j)$ and $\Theta(j+1)$ is calculated:

$$A_M(j) = 2\pi R_{pl}^2 (\sin(\Theta(j+1) - \sin(\Theta(j)) \,. \tag{7}$$

Next, this area is distributed evenly among all planet cells within $\Theta(j)$ and $\Theta(j+1)$ by

$$A_{C,pl}(i,j) = A_M(j)/n_{Phi} \,. \tag{8}$$

Starting conditions and numerical integration

The satellite and planet starting conditions can either be specified as a state vector (position and velocity in Cartesian space) or by means of Keplerian elements. If Keplerian elements are specified, the starting state vectors of planet and spacecraft $\vec{P}$ (position) and $\vec{V}$ (velocity) are given by the transformations

$$\vec{P} = r \begin{bmatrix} \cos(\omega+\nu)\cos\Omega - \sin(\omega+\nu)\sin\Omega\cos i \\ \cos(\omega+\nu)\sin\Omega + \sin(\omega+\nu)\cos\Omega\cos i \\ \sin(\omega+\nu)\sin i\,, \end{bmatrix} \tag{9}$$

$$\vec{V} = \sqrt{\frac{\mu}{p}}\, e \sin\nu\vec{P} + \frac{\sqrt{\mu\, p}}{r} \cdot \begin{bmatrix} -\sin(\omega+\nu)\cos\Omega - \cos(\omega+\nu)\sin\Omega\cos i \\ -\sin(\omega+\nu)\sin\Omega + \cos(\omega+\nu)\cos\Omega\cos i \\ \cos(\omega+\nu)\sin i\,, \end{bmatrix} \tag{10}$$

where $\mu = G\, M_B$ with the gravitational constant G and the mass of the orbited central body M_B and

$$r = \frac{p}{1 + e\cos\nu}\,, \tag{11}$$

where $p = a(1-e^2)$. Note that state vector information is always given within the inertial frame, in which the Keplerian elements are defined. Consequently, $\vec{P}$ and $\vec{V}$ are given in MCI-coordinates for the spacecraft and in HCI coordinates for the planet. Starting from these state vectors, the orbits of planet and spacecraft are integrated numerically by the two-body equation

$$\vec{P}(t) = \vec{P}(t_0) + \mu \int\int -\frac{1}{r^3} \cdot \vec{r}\, dtdt\,, \tag{12}$$

where t_0 is the starting time, μ is the specific gravitational constant of the orbited body and r is the position vector of the orbiting body. Within GENERIC this computation is realized by means of SIMULINK integration blocks with starting conditions $\vec{P}(t_0)$ and $\vec{V}(t_0)$. Since the disturbance analysis demands transformations between the different coordinate systems, which are defined by means of Keplerian elements, the calculated state vectors have to be re-transformed into Keplerian elements for each time step. By this approach, the spacecraft position in the planet frame can be updated corresponding to the current position of the planet. The calculation of the Keplerian elements uses the known planet position $\vec{r}_{pl,HCI}$ and the planet velocity vector $\vec{v}_{pl,HCI}$ in inertial space. The specific angular momentum can be obtained from

$$\vec{h}_{pl,HCI} = \vec{r}_{pl,HCI} \times \vec{v}_{pl,HCI}\,. \tag{13}$$

The eccentricity vector, which results from the integration of the specific angular momentum vector, is defined as

$$\vec{e}_{pl} = \frac{1}{\mu} \cdot \vec{v}_{pl,HCI} \times \vec{h}_{pl,HCI} - \frac{\vec{r}_{pl,HCI}}{|\vec{r}_{pl,HCI}|}\,. \tag{14}$$

The eccentricity can then be calculated by $e_{pl} = |\vec{e}_{pl}|$. The right ascension Ω_{pl} is known from the angular momentum vector $\vec{h}_{pl,HCI}$ by

$$\Omega_{pl} = \arctan\left(\frac{h_1}{-h_2}\right)\,, \tag{15}$$

where h_1 and h_2 are the x_{HCI} and y_{HCI} components of $\vec{h}_{pl,HCI}$, respectively. The inclination i_{pl} is given by

$$i_{PL} = \arccos\left(\frac{h_3}{|\vec{h}_{pl,HCI}|}\right)\,, \tag{16}$$

where h_3 is the z_{HCI} component of $\vec{h}_{pl,HCI}$. With the orbit parameter

$$p = \frac{|\vec{h}_{pl,HCI}|^2}{\mu}\,, \tag{17}$$

the semi major axis a can be determined to

$$a = \frac{p}{(1 - e_{pl}^2)}\,. \tag{18}$$

The true anomaly can be computed from

$$\nu_{pl} = \arccos\left(\frac{\vec{e}_{pl} \cdot \vec{r}_{pl}}{|\vec{e}_{pl} \cdot \vec{r}_{pl}|}\right)\,. \tag{19}$$

Finally the argument of periapsis follows from

$$\omega = \arccos\left(\frac{\vec{e}_{pl} \cdot \vec{n}_{pl}}{|\vec{e}_{pl} \cdot \vec{n}_{pl}|}\right)\,, \tag{20}$$

where $\vec{n}_{pl}$ is the periapsis vector

$$\vec{n}_{pl} = \begin{pmatrix}0\\0\\1\end{pmatrix} \times \vec{h}_{pl,HCI}\,. \tag{21}$$

By deriving the Keplerian elements of the planet for each time step and using the transformations defined in the frame definition section, the simulation includes the change of planet position while the spacecraft orbits the planet. The resulting effect can be seen from the evolution of the spacecraft position for one orbit rotation, expressed in planet frame. As shown in figure 4, the spacecraft orbit slowly rotates in the planet frame, summing up to one full rotation for a whole planet year. Note that the same calculation can be performed to obtain the updated Keplerian elements of the spacecraft. In this case, Mercury has to be regarded as the central body, implying the use of the Mercury-specific gravitational constant instead of the solar gravitational constant.

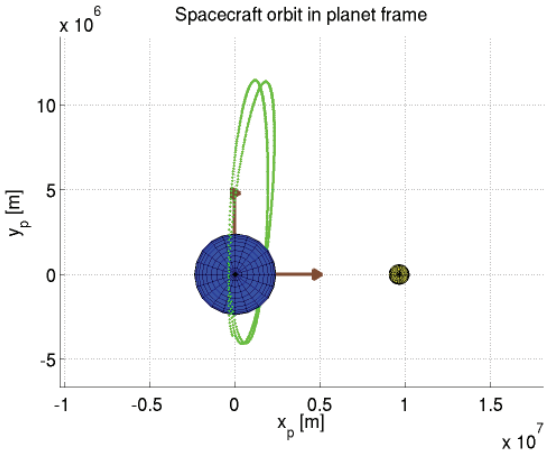

Figure 4. Rotation of orbital plane in PL frame during the course of two orbits

SRP Model

The SRP acting on the different spacecraft surfaces is determined by the direction to the sun, the solar distance as well as the position of the planet and the optical properties of the spacecraft surfaces. The solar flux at the spacecrafts distance from the sun $r_{sc,HCI}$ can be determined with

$$P(r_{sc}) = \frac{P_{1AU}}{|\vec{r}_{sc,HCI}|^2}\,. \tag{22}$$

The total acceleration acting on each individual spacecraft cell k can then be computed with

$$\vec{a}_{SRP,SC}(k) = \frac{P(r_{sc,HCI})}{c \cdot m_{sc}} A_{sc}(k) \cos\phi_{inc} \Bigg[(\alpha_{sc}(k) + \gamma_{D,sc}(k)) \cdot \vec{r}_{sun,SC} + 2\left(\frac{\gamma_{D,sc}(k)}{3} + \gamma_{S,sc}(k)\cos\phi_{inc}\right)\Bigg] \vec{n}_{sc,SC}(k)\,, \tag{23}$$

where m_{sc} is the spacecrafts mass, $\vec{r}_{sun,SC}$ is the sun direction in SC frame, ϕ is the angle of incidence of the incoming sunlight and $\vec{n}_{sc,SC}(k)$ is the surface normal on each spacecraft cell, expressed in SC frame. Only cells, where $\phi_{inc} = \arccos\left(\vec{n}_{sc,SC}(k) \cdot \vec{r}_{sun,SC}\right) \leq \pi/2$ and which are not in eclipse, are subjected to SRP. The total SRP can then be determined by summing all individual SRP results. The GENERIC eclipse model is displayed in figure 5.[8]

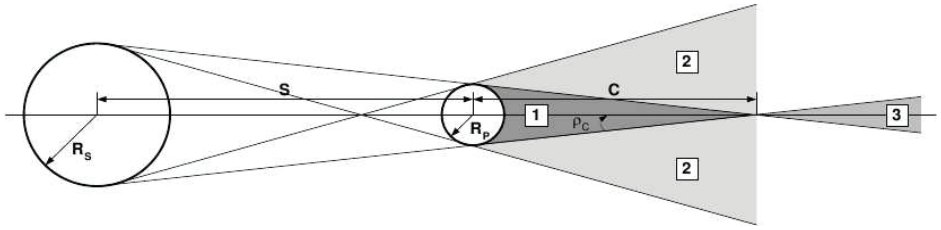

Figure 5. Different types of eclipses

The length of the shadow C can be determined by

$$C = \frac{R_{pl} S}{R_{sun} - R_{pl}}\,, \tag{24}$$

where S is the distance of the planet to the sun with $S = |\vec{r}_{pl,HCI}|$ and R_{pl} and R_{sun} are the radii of the planet and sun, respectively. The angle Θ between the vector from the spacecraft to the sun $\vec{D}_S = -r_{sc,HCI}$ and the vector from the spacecraft to the planet $\vec{D}_P = -r_{sc,PL}$ is

$$\Theta = \arccos(\vec{D}_S \cdot \vec{D}_P)\,. \tag{25}$$

The apparent angular radii of sun and planet, as viewed from the spacecraft can be expressed as

$$\rho_S = \arcsin(\frac{R_S}{D_S}) \;\text{ and }\; \rho_P = \arcsin(\frac{R_P}{D_P})\,, \tag{26}$$

where $D_S = |\vec{r}_{sc,HCI}|$ and $D_P = |\vec{r}_{sc,PL}|$ are the distances of the spacecraft to the sun and to the planet center, respectively. The different types of possible eclipses can then be formulated as

1: Total eclipse:	$S < D_S < S + C$ and $\rho_P - \rho_S > \Theta$
2: Partial eclipse:	$D_S > S$ and $\rho_P + \rho_S > \Theta > \lvert\rho_P - \rho_S\rvert$
3: Annular eclipse:	$S + C < D_S$ and $\rho_P - \rho_S > \Theta$

If either of the eclipses is detected, the received solar flux for all spacecraft cells is set to zero, effectively leading to no SRP acting on the spacecraft during eclipse.

INF Model

For the calculation of the influence of infrared radiation (as well as for ALB and TRP) the interaction between planet surface and spacecraft surfaces determines the magnitude of the resulting perturbations. Consequently, an illumination model, which determines which planet cells are illuminated by the sun and thus specifies the cell surface temperature is necessary. Furthermore, a visibility model, which determines the fraction of the planet surface that exchanges radiation with each of the spacecraft surfaces, is needed. The illumination model is illustrated in figure 6.

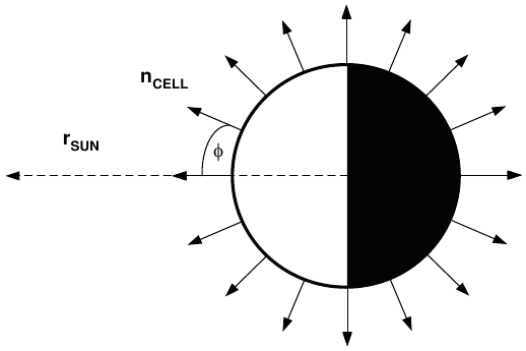

Figure 6. Illumination model

The criterion for an illuminated planet cell can be formulated by means of the illumination angle $\phi_{ILLU}(i,j)$ with

$$\phi_{ILLU}(i,j) = \arccos(\vec{r}_{sun,PL} \cdot \vec{n}_{pl,PL}(i,j)) \leq \frac{\pi}{2}, \tag{27}$$

where $\vec{n}_{pl,PL}(i,j)$ is the respective normal vector on the planet cell surface and $\vec{r}_{sun,PL}$ is the sun vector in planet frame. As can be seen in figure 7 for an exemplary spacecraft and planet constellation, the visibility of any planet cell to a spacecraft cell depends on the orientation of the different spacecraft cells as well as on the position of the spacecraft with respect to the planet cells as shown in figure 7.

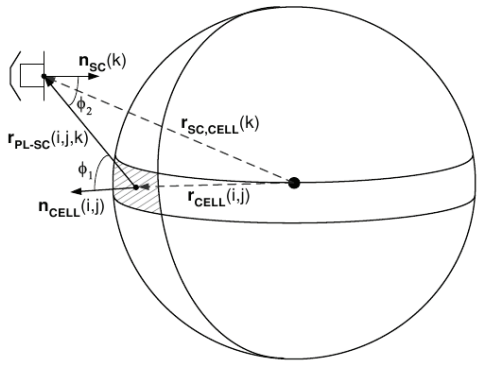

Figure 7. Visibility model

The line of sight vector from a planet cell to a spacecraft cell $\vec{r}_{pl-sc,PL}(i,j,k)$ is defined as

$$\vec{r}_{pl-sc,PL}(i,j,k) = \vec{r}_{C,sc,PL}(k) - \vec{r}_{C,pl,PL}(i,j)\,, \tag{28}$$

where $\vec{r}_{C,sc,PL}(k)$ is the position of the spacecraft surface centers expressed in the planet frame. Two visibility angles can be defined:

$$\phi_{VIS,1}(i,j,k) = \arccos(\vec{r}_{pl-sc,PL}(i,j,k) \cdot \vec{n}_{C,pl,PL}(i,j))\,, \tag{29}$$

$$\phi_{VIS,2}(i,j,k) = \arccos(-\vec{r}_{pl-sc,PL}(i,j,k) \cdot \vec{n}_{sc,PL}(k))\,, \tag{30}$$

where $\vec{n}_{SC}(k)$ is the normal vector of spacecraft surface k. A planet cell (i,j) is visible to a spacecraft cell k if

$$\phi_{VIS,1}(i,j,k) \leq \frac{\pi}{2} \text{ and } \phi_{VIS,2}(i,j,k) \leq \frac{\pi}{2}\,. \tag{31}$$

Since the magnitude of infrared radiation depends on the planet surface temperature, the mean temperatures of the planet surface cells visible to the spacecraft cells have to be determined. This is realized by a twofold approach. For the "night" side of the planet a fixed "night" temperature is applied to all planet cells which are not illuminated by the sun. On the "day" side the temperature is then calculated by means of the thermal equilibrium between incoming solar radiation and outgoing radiation emitted by the planet surface. Here the total receiving projected area $A_{rec,pl} = \pi(R_{pl})^2$ is only half of the emitting surface area $A_{day,pl} = 2\pi(R_{pl})^2$, leading to

$$T_{day,pl} = \left(\frac{P_{1AU}}{r_{pl,HCI}^2} \alpha_{pl}(i,j) \frac{1}{2\sigma\varepsilon_{pl}(i,j)} \right)^{\frac{1}{4}}\,. \tag{32}$$

Note that this approach does not include thermal gradients and assumes constant temperatures on either of the planet sides.

The magnitude of the radiation flux from any visible planet cell (i,j) to a spacecraft cell k is characterized by the radiation view factor $F(i,j,k)$

$$F(i,j,k) = \frac{\cos\phi_{VIS,1}\cos\phi_{VIS,2}}{\pi|\vec{r}_{pl-sc,PL}(i,j,k)|^2} A_{sc}(k)\,, \tag{33}$$

which is a simplification of the exact radiation view factor integral as it is valid only for large distances (compared to the surface dimensions) between spacecraft and planet surface cells. The total emitted planet cell energy E_{pl} can be calculated with

$$E_{pl}(i,j) = \sigma\varepsilon_{pl}(i,j) A_{pl}(i,j) T_{pl}(i,j)^4\,. \tag{34}$$

The radiation flux received by a spacecraft cell k is then characterized by

$$E_{INF}(i,j,k) = E_{pl}(i,j) \cdot F(i,j,k)\,. \tag{35}$$

Now the INF acceleration resulting from emission of planet cell i,j into spacecraft cell k can be computed by

$$\begin{aligned} \vec{a}_{INF,SC}(i,j,k) = \frac{E_{INF}(i,j,k))}{c \cdot m_{sc}} \Bigg[& (\alpha_{sc}(k) + \gamma_{D,sc}(k)) \cdot (-\vec{r}_{sc,pl,SC}(k)) \\ & + 2\left(\frac{\gamma_{D,sc}(k)}{3} + \gamma_{S,sc}(k)\cos\phi_{VIS,2}(i,j,k) \right) \Bigg] \vec{n}_{sc,SC}(k)\,. \end{aligned} \tag{36}$$

The total INF acting on the spacecraft is then calculated by summing all individual $\vec{a}_{INF,SC}(i,j,k)$ over all planet and all spacecraft cells.

ALB Model

The calculation of the ALB acting on the spacecraft is realized in a twofold approach. First the solar flux received by the individual planet cells is calculated. Based on the planet cell optical properties the reflected fluxes and the fluxes received by the spacecraft cells are then obtained. The second step closely resembles the calculation of the INF. The received solar flux $P_{rec,pl}(i,j)$ is determined by the orientation of each planet cell i,j to the sun with

$$P_{rec,pl}(i,j) = \frac{P_{1AU}}{r_{pl,HCI}^2} \cos\phi_{sun}(i,j)\,, \tag{37}$$

where the sun orientation angle $\phi_{sun}(i,j)$ of each cell is characterized by

$$\phi_{sun}(i,j) = \arccos(\vec{n}_{pl}(i,j) \cdot \vec{r}_{sun})\,. \tag{38}$$

Note that only the illuminated cells (see INF model description) are considered in this approach. The total energy reflected by the planet cell can then be computed by

$$E_{refl,pl}(i,j) = \gamma_{D,pl}(i,j) P_{rec,pl}(i,j) A_{pl}(i,j)\,. \tag{39}$$

Assuming a perfect diffuse reflection of the incoming solar radiation, the energy received by a spacecraft cell k can be determined by means of view factors $F(i,j,k)$, as described in the INF model section

$$E_{ALB}(i,j,k) = F(i,j,k) E_{refl,pl}(i,j)\,. \tag{40}$$

Corresponding to the INF visibility model , spacecraft surfaces only receive Albedo from those planet cells which are visible to the spacecraft. In conclusion, the ALB acceleration acting on spacecraft surface k caused by solar radiation reflected by a visible and illuminated planet surface i,j is

$$\begin{aligned}\vec{a}_{ALB,SC}(i,j,k) = \frac{E_{ALB}(i,j,k))}{c \cdot m_{sc}} \Bigg[& (\alpha_{sc}(k) + \gamma_{D,sc}(k)) \cdot (-\vec{r}_{pl-sc,SC}(k)) \\ & + 2\left(\frac{\gamma_{D,sc}(k)}{3} + \gamma_{S,sc}(k)\cos\phi_{VIS,2}(i,j,k)\right)\Bigg] \vec{n}_{sc,SC}(k)\,.\end{aligned} \tag{41}$$

The sum over all planet and spacecraft cells then delivers the total spacecraft ALB acceleration.

TRP Model

The TRP model is the most complex perturbation model within the GENERIC tool, since the TRP magnitude depends on SRP, INF and ALB information. Consider a spacecraft in the vicinity of a planet as depicted in figure 8.

Assuming thermal equilibrium, the resulting spacecraft surface temperatures depend on the magnitude of the incoming albedo, solar and infrared radiation fluxes. In addition an internal heat generation as well as heat transfer through the spacecraft interior volumes and into the space environment (by means of heat radiation) has to be considered. The general heat balance can be formulated as

$$Q_{out} = Q_{Gen} + Q_{rec,SUN} + Q_{rec,INF} + Q_{rec,ALB}\,, \tag{42}$$

where Q_{out} is the heat flux emitted by the spacecraft surface, Q_{Gen} is internal heat production and $Q_{rec,SUN}$, $Q_{rec,INF}$ and $Q_{rec,ALB}$ are the received solar, infrared and albedo heat fluxes, respectively. For missions close to the sun, the internally generated energy is negligible compared to the

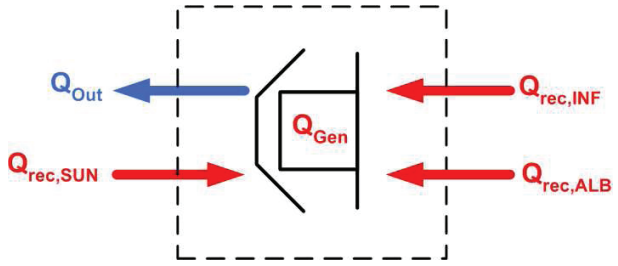

Figure 8. Heat balance for spacecraft system

incoming energy fluxes. Furthermore heat conduction into other parts of the spacecraft doesn't need to be treated in case of good insulation, as is usually the case for bus and heat shield surfaces. Consequently the heat balance simplifies and the equilibrium temperature of spacecraft surface k becomes

$$T_e(k) = \left(\frac{Q_{rec,SUN}(k) + Q_{rec,INF}(k) + Q_{rec,ALB}(k)}{\sigma \varepsilon_{sc}(k) A(k)} \right)^{\frac{1}{4}}, \tag{43}$$

where σ is Stefan-Boltzmann's constant, $\varepsilon_{sc}(k)$ is the spacecraft surface emissivity with $\varepsilon_{sc}(k) = \alpha_{sc}(k)$ and the outgoing heat flux can be described by Stefan Boltzmann's law $Q_{out} = \sigma \varepsilon_{sc} A T_e^4$. For thin structures such as solar panels, where the through-thickness heat conduction may significantly affect the resulting equilibrium temperatures, a different approach has to be taken. Considering a standard solar panel geometry (honeycomb core with face sheets) as shown in cross-section in figure 9, two energy balances (one for the front and one for the rear) may be formulated.

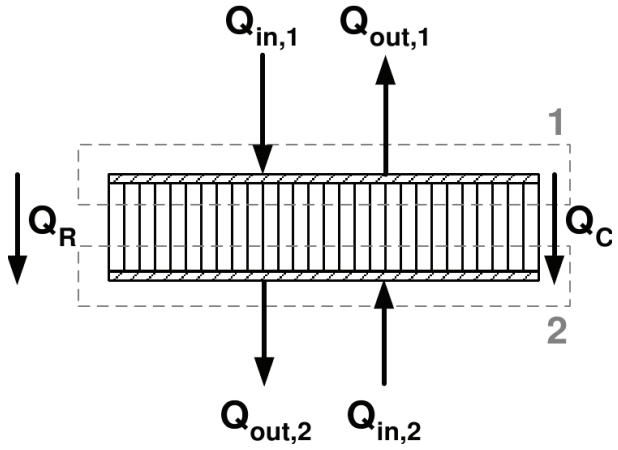

Figure 9. Incoming and outgoing heat fluxes for a standard solar panel

$$\begin{aligned} Q_{in,1} - Q_R - Q_C - Q_{out,1} &= 0\,, \\ Q_{in,2} + Q_R + Q_C - Q_{out,2} &= 0\,, \end{aligned} \tag{44}$$

where $Q_{in,1}$ and $Q_{in,2}$ are the external heat fluxes received by the front and rear of the solar panel, $Q_{out,1}$ and $Q_{out,2}$ are the re-emitted heat fluxes. The heat transport through the array is governed by

two different effects. A considerable amount of heat Q_R is transported through the honeycomb core by heat radiation, resulting from the fact that the individual honeycomb cells only possess a small cross-sectional area for heat conduction. Heat Q_C is also conducted directly through the honeycomb material. The ratio Q_C/Q_R is determined by the geometric and optical properties of the honeycomb core. The model presented here has been established by a study of the Rosetta spacecraft.[9]

The mean thermal conductivity q_{SP} can be calculated by

$$q_{SP} = \frac{k_{SP}}{d_{SP}} r_{HC} r_C \,, \tag{45}$$

where k_{SP} is the thermal conductivity of the solar panel core material, d_{SP} is the thickness of the solar panel, r_{HC} is the ratio of honeycomb cell cross-sectional area to the panel area and r_C the solar cell packing factor. The heat transported by heat conduction is

$$Q_C = q_{SP} \Delta T = q_{SP}(T_1 - T_2) \,, \tag{46}$$

where T_1 and T_2 are the front and rear temperatures, respectively. The radiative heat transport can be expressed as

$$Q_R = \varepsilon_{int} \sigma \frac{1 - r_{HC}}{2 - \varepsilon_{int}} (T_1^4 - T_2^4) \,. \tag{47}$$

In order to compute the equilibrium temperatures, equation 44 has to be solved iteratively. To accomplish this, starting values $\overline{T}_1$ and $\overline{T}_2$ are computed by

$$\overline{T}_1 = \left(\frac{Q_{in,1}}{\sigma A \varepsilon_1} \right) \text{ and } \overline{T}_2 = \left(\frac{Q_{in,2}}{\sigma A \varepsilon_2} \right) . \tag{48}$$

The solution of the equation system

$$\begin{aligned} Q_{in,1} - \varepsilon_{int} \sigma \frac{1 - r_{HC}}{2 - \varepsilon_{int}} (T_1^4 - T_2^4) - q_{SP} \Delta T = q_{SP}(T_1 - T_2) - \sigma \varepsilon_1 A_1 T_1^4 &= 0 \,, \\ Q_{in,2} + \varepsilon_{int} \sigma \frac{1 - r_{HC}}{2 - \varepsilon_{int}} (T_1^4 - T_2^4) + q_{SP} \Delta T = q_{SP}(T_1 - T_2) - \sigma \varepsilon_2 A_2 T_2^4 &= 0 \,, \end{aligned} \tag{49}$$

with starting values $\overline{T}_1$ and $\overline{T}_2$ delivers the equilibrium temperatures. Note that for higher precision, the optical properties of the interior and exterior surfaces of the panel may also be modeled as a function of the actual surface temperature.

By assigning the iterated temperatures to the respective spacecraft solar panel cells k, the spacecraft surface equilibrium temperature set $T_e(k)$ can now be computed and the TRP acceleration acting on each spacecraft surface cell can be calculated with

$$\vec{a}_{TRP,SC}(k) = -\frac{2}{3 m_{sc} c} \vec{n}_{sc,SC}(k) \sigma \varepsilon_{sc}(k) A_{sc}(k) T_{sc}(k)^4 \,, \tag{50}$$

where the factor 2/3 results from Lambert's cosine law and the hemispheric emission pattern. The total TRP can be computed by the sum of all individual spacecraft surface cell TRP vectors.

SPACECRAFT AND MISSION SCENARIO

As an example test and evaluation case the Messenger mission has been chosen for a detailed analysis of solar and thermal perturbations. The evaluation of these perturbations acting on the Messenger spacecraft demands the simulation of the spacecraft trajectory for a whole Mercury year as well as the detailed investigation of specific scenarios. The initial orbit is specified to the measured initial Messenger MOI-values as given in Stanbridge et al.[10] The resulting orbital elements in inertial MCI frame are listed in table 3. The mean orbital elements of Mercury, which are used in this study are specified in table 4.

Table 3. Messenger orbital elements in MCI coordinates

Semi-major axis [m]	Eccentricity [-]	Right Ascension [°]	Inclination [°]	Argument of Periapsis [°]
10175000	0.74	350.17	82.52	119.16

Table 4. Mercury MOI orbital elements in HCI coordinates

Semi-major axis [m]	Eccentricity [-]	Right Ascension [°]	Inclination [°]	Argument of Periapsis [°]
57910000000	0.2056	48.33	7.0	77.46

A parameter constellation constructed from the freely available information[10] has been chosen as test case for the analysis. These reference values are listed in table 5.

Table 5. Messenger model parameters

Cell area [m^2]	Right ascension [°]	Declination [°]	Cell center [m]	α_{sc}	$\gamma_{S,sc}$	$\gamma_{D,sc}$
2.122	-127.2	0.0	[-0.71 -1.2125 0.0]	0.64	0.14	0.22
1.264	-90.0	0.0	[0.0 -1.0 0.0]	0.63	0.14	0.23
2.121	-52.8	0.0	[0.71 -1.2125 0.0]	0.64	0.14	0.22
2.35	0.0	0.0	[0.71 0.0 0.0]	0.7	0.05	0.25
2.35	180.0	0.0	[-0.71 0.0 0.0]	0.7	0.05	0.25
1.803	0.0	90.0	[0.0 0.0 0.635]	0.7	0.05	0.25
1.803	0.0	-90.0	[0.0 0.0 -0.635]	0.7	0.05	0.25
4.612	90.0	0.0	[0.0 0.925 0.0]	0.7	0.05	0.25
2.724	-90.0	0.0	[1.943 0.0 0.0]	0.75	0.25	0.0
2.724	-90.0	0.0	[-1.943 0.0 0.0]	0.75	0.25	0.0
2.724	90.	0.0	[1.943 0.0 0.0]	0.7	0.05	0.25
2.724	90.	0.0	[-1.943 0.0 0.0]	0.7	0.05	0.25

The resulting Messenger spacecraft model is displayed in figure 10. The scope of the analysis is i) the evaluation of the numerical method by means of the analytical method introduced in Ref.[6] as well as ii) the analysis of the thermal perturbations acting on the Messenger spacecraft for a complete Mercury year, including the different trajectories of both planet and spacecraft. Hence, the following section compares results obtained with the analytical method to the numerical results for defined test scenarios.

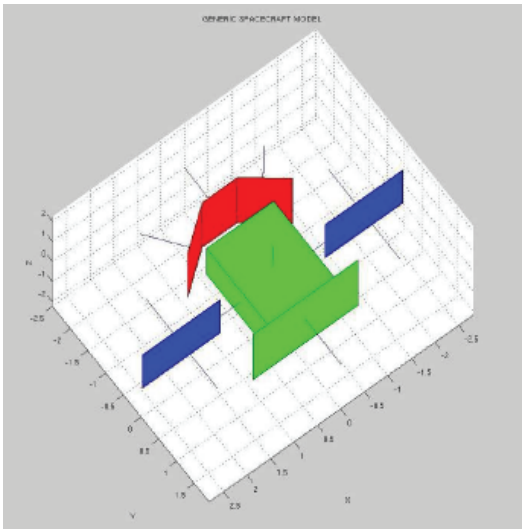

Figure 10. Spacecraft model: Messenger example.

EVALUATION WITH ANALYTICAL RESULTS

Test Case Parameters

The presented numerical model has been evaluated for the Messenger orbit by comparing with the analytical model previously developed.[6] There are relevant works already published on the orbit determination and modeling of Messenger spacecraft.[7,10] However, these papers have no provision for thermal re-radiation effects (i.e. TRP) which are expected to have considerable effects under the severe flux from the Sun near Mercury. It is important to note that the present numerical and analytical models have been developed independently including the temperature calculations and thus, the proposed approach is appropriate for evaluation purposes.

We implement the parameters achieved by Messenger as our test cases for the practical illustration,[11,12] see Figure 11 and Table 6. Test cases are shown in Figure 11 with respective distance of Mercury from Sun and orbit plane orientation of the orbiter at each position. These test cases are representing unique geometries under the heliocentric progression of Mercury. In particular, the orbit plane of the orbiter aligns close to the terminator (Dawn-Dusk orbit) in Case 1 and 3 and it passes over the sub-solar point (Noon-Midnight orbit) in Case 2 and 4. At each test case condition, we calculate non-gravitational perturbations over one revolution of the orbiter (i.e. 12 hours).

Table 6. Test case parameters of Mercury and Orbiter

Case No.	ν_M [deg]	Ω_{SC} [deg]
1	10	350
2	98	
3	189	
4	279	

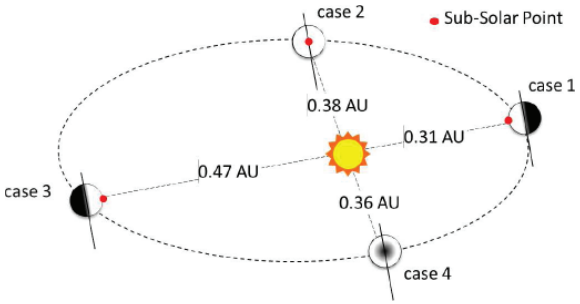

Figure 11. Evaluation test cases

For these four cases shown in Figure 11, a few of the orbital elements of the orbiter are fixed, in particular semi-major axis, eccentricity, argument of periapsis, and inclination. These parameters are set to the MOI values achieved by Messenger,[12] see Table 3. Table 4 contains the parameters of Mercury. Note that all orbital elements of the orbiter in Table 3 are defined in the MCI frame.[13]

Analytical Model

The model evaluation has been performed by using the analytical model developed by the authors.[6] These prescribed cases have advantages because of their unique geometries, so that relative positions can be obtained analytically by means of straightforward procedures.[6]

Perturbation equations are identical in the numerical and analytical model, however there are several aspects which are not taken into account for the analytical model, e.g. the 7 [deg] inclination of the Mercury orbit plane. Note that the solar flux is assumed to be uniformly parallel in the analytical model and thus, the eclipse by Mercury is calculated with a cylindrical model.[6] In addition, the Mercury surface cell area calculation method used in the numerical model is implemented into the analytical model, see 8. It is important to note that the view factor calculation is still valid even though we modified the area calculation method. In short, the major assumptions and conditions applied in the analytical model are summarized as follows;

- Evolution and rotation of Mercury are neglected during one evolution of the orbiter (12 hrs),
- The orbiter follows the Keplarian motion around Mercury.

Comparison and Evaluation

Independent results obtained from the two models are evaluated in the prescribed test cases. Tables 7 and 8 contain the magnitude of the SRP effect in each case and the percentages of each perturbation with respect to SRP. We note that in the analytical model, Mercury's orbital motion is not taken into account and thus the magnitude of SRP is fixed except eclipses.

There are several differences to be found in the results shown in Tables 7 and 8. These discrepancies are induced by the progression of the orbit plane of the orbiter. In the analytical model, the orbit plane is fixed during the simulation, on the other hand in the numerical model, the orbit plane is shifted about 2 [deg] in terms of right ascension after one orbit. This displacement induces the difference in the peaks, however the average magnitudes of each perturbation stays below 5 percent.

Table 7. Analytical Results of Acceleration in [%] of SRP Magnitude

		ALB [% of SRP]		INF [% of SRP]		TRP [% of SRP]	
Case	SRP [10^{-7}m/s^2]	max	min	max	min	max	min
1	8.45	0.32	0.02	6.68	0.18	25.60	23.44
2	5.51	2.37	0.00	14.10	0.01	23.24	18.80
3	3.71	0.95	0.01	19.24	0.14	19.99	18.81
4	6.22	6.45	0.00	26.79	0.00	24.05	17.93

Table 8. Numerical Results of Acceleration in [%] of SRP magnitude

Case	SRP [10^{-7}m/s^2]		ALB [% of SRP]		INF [% of SRP]		TRP [% of SRP]	
	max	min	max	min	max	min	max	min
1	8.45	8.42	0.20	0.00	3.66	0.17	23.78	23.31
2	5.51	(eclipse)	4.40	0.00	25.22	0.02	20.43	18.46
3	3.72	3.71	0.77	0.01	17.56	0.08	18.97	16.89
4	6.33	(eclipse)	6.11	0.00	25.70	0.00	21.33	17.74

Furthermore, the magnitudes of the accelerations of SRP, INF, ALB are at the approximate magnitudes given in Ref.[10] These results confirm that the models are practically appropriate and they provide further insight in the characteristics of the thermal effects.

NUMERICAL RESULTS

The evolution of the magnitudes of SRP, INF, ALB, and TRP acting on a Messenger-like spacecraft has been analyzed by using the mission and spacecraft parameters listed in tables 4, 3 and 5. The magnitude of the perturbations has been computed for the test cases defined in the previous section. Results for the different perturbations are shown in figure 12.

As can be seen, all disturbance magnitudes are proportional to the inverse square of the distance to the sun. The SRP is the dominant disturbance in all cases, followed by TRP, INF and ALB. The thermal effects show peaks in the vicinity of the planet, which is understandable, since the view factors to the planet surface scale with the inverse square of the distance of the spacecraft to the planet. In total, the mean sum of all thermal effects stays in the range of 20-30 % of the SRP. Near the planet surface peak values show higher percentages, as listed in table 8.

For a complete evaluation of the solar and thermal perturbations acting on Messenger a complete Mercury year, implying 172 spacecraft orbits, has been processed. The computed evolution of the maximum perturbations are shown in figure 13 with respect to Mercury's true anomaly. As can be seen, SRP is the dominant effect, INF and TRP maximum values are in the order of 25 % of the SRP and ALB is mostly negligible. Since TRP, INF and ALB increase for Mercury true anomalies above 180^o, the sum of all thermal effects can be up to 50 % of the SRP. In total a maximum disturbance in the order of μm/s^2 results from the sum of all solar and thermal effects. Note that these results are highly dependent on the spacecraft and planet orbits since in particular the evolution of the thermal forces depends on the orientation of the spacecraft to the planet terminator.

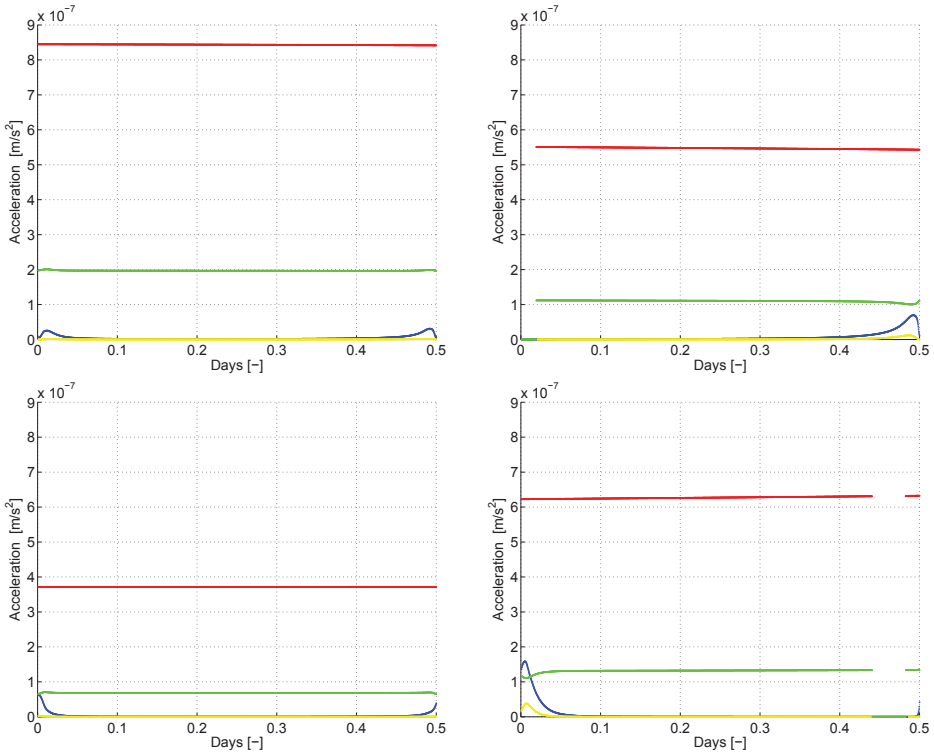

Figure 12. Numerical results for perturbations in evaluation test cases. Upper left: $\omega_{pl} = 10^{o}$, Upper right: $\omega_{pl} = 98^{o}$, Lower left: $\omega_{pl} = 189^{o}$, Lower right: $\omega_{pl} = 279^{o}$ Red: SRP, Blue: INF, Yellow: ALB, Green: TRP

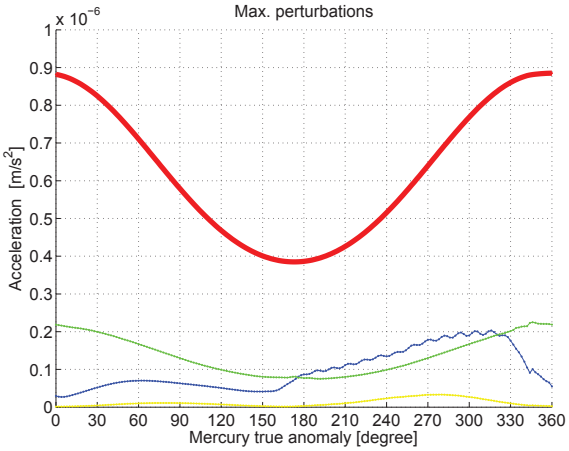

Figure 13. Numerical results for maximum disturbances acting on Messenger during Mercury year. Red: SRP, Blue: INF, Yellow: ALB, Green: TRP

CONCLUSION

In this paper a new numerical method for the analysis of thermal perturbations acting on spacecraft surfaces has been introduced. For specific test cases the resulting perturbation magnitudes have been compared to analytical solutions. By this, the performance of the numerical methods has been evaluated. The evolution and magnitude of SRP, INF, ALB and TRP has been analyzed in detail for specific configurations of planet and spacecraft. Furthermore the evolution of the mean perturbations (averaged over one spacecraft orbit) as well as the minimum and maximum values have been computed for a full Mercury year. Results show that for close distances to planet and sun the sum of the treated perturbations reach μm/s^2 magnitude. With a spacecraft mass of $m_{sc} = 700\,\text{kg}$ this leads to a total perturbation force of 10^{-4} N magnitude, which has a significant influence on the spacecraft trajectory.

The modelling method introduced in this paper can be used for any spacecraft architecture orbiting any planet within the solar system. Due to the cell approach, spacecraft and planet modelling accuracy is greatly improved with respect to analytical approaches. Hence, the feasible modelling accuracy is mainly limited by the available computational power but not by the approach itself. Furthermore, the numerical integration of the trajectories of both planet and spacecraft enables the inclusion of the computed perturbations as disturbance accelerations on the calculated trajectory thus changing the Keplerian elements over time. In conclusion, the GENERIC model provides a powerful tool for the analysis of the effects of solar and thermal perturbations on spacecraft orbits.

REFERENCES

[1] B. Rievers and C. Lämmerzahl, "High Precision Thermal Modeling of Complex Systems with Application to the Flyby and Pioneer Anomaly," *Annalen der Physik*, Vol. 523, No. 6, 2011, pp. 439–449, 10.1002/andp.201100081.

[2] T. Kato, B. Rievers, J. C. van der Ha, and C. Lämmerzahl, "Detailed Analysis of Solar and Thermal Accelerations on Deep-Space Satellites," *Advances in the Astronautical Sciences*, Vol. 143, 2012, pp. 1761–1776.

[3] B. Rievers, T. Kato, J. C. van der Ha, and C. Lämmerzahl, "Numerical Prediction of Satellite Surface Forces with Application to Rosetta," *Advances in the Astronautical Sciences*, Vol. 143, 2012, pp. 1123–1142.

[4] T. Kato and J. C. van der Ha, "Precise Modeling of Solar and Thermal Accelerations on Rosetta," *Acta Astronautica*, Vol. 72, 2012, pp. 165–177.

[5] M. Shoemaker, J. C. van der Ha, and T. Morley, "Modeling and Validation of Thermal Radiation Acceleration on Interplanetary Spacecraft," *Journal of Spacecraft and Rockets*, Vol. 49, 2012, pp. 212–219.

[6] T. Kato, B. Rievers, J. C. van der Ha, and C. Lämmerzahl, "Sensitivity Analysis of the Non-Gravitational Perturbations on a Mercury Orbiter," *Advances in the Astronautical Sciences*, Vol. 143, February 2012, pp. 1579 – 1595.

[7] C. J. Scott, J. V. McAdams, D. P. Moessner, and C. Ercol, "Modeling The Effects of Albedo and Infrared Radiation Pressures on The MESSENGER Spacecraft," *Advances in the Astronautical Sciences*, Vol. 142, 2012. AAS 11-552.

[8] J. R. Wertz, *Spacecraft Attitude Determination and Control*. The Netherlands: Kluwer Academic Publishers, 1978.

[9] J. C. van der Ha and D. Stramaccioni, "Thermal Radiation Effects on Deep-Space Trajectories," *Advances in the Astronautical Sciences*, Vol. 136, 2010, pp. 1861 – 1880.

[10] D. R. Stanbridge, K. E. Williams, A. H. Taylor, B. R. Page, C. G. Bryan, and D. W. Dunham et al., "Achievable Force Model Accuracies for MESSENGER in Mercury Orbit," *Advances in the Astronautical Sciences*, Vol. 142, 2012. AAS 11-548.

[11] S. C. Solomon, R. L. McNutt, R. E. G. Jr., and D. L. Domingue, "MESSENGER Mission Overview," *Space Science Review*, Vol. 131, 2007, pp. 3 – 39.

[12] D. P. Moessner and J. V. McAdams, "The MESSENGER Spacecraft's Orbit-Phase Trajectory," *Advances in the Astronautical Sciences*, Vol. 142, 2012. AAS 11-547.

[13] JPL, "HORIZONS System," webpage. http://ssd.jpl.nasa.gov/?horizons.